Application of a multi-phase multi-morphology crystallization model to isotactic polypropylenes with different molecular weight distributions

European Polymer Journal 97 (2017) 397–408

Contents lists available at ScienceDirect

European Polymer Journal

journal homepage: www.elsevier.com/locate/europolj

Application of a multi-phase multi-morphology crystallization model to isotactic polypropylenes with different molecular weight distributions

E.M. Troisi[a,b,1], S.A.J.J. Arntz[a], P.C. Roozemond[c], A.H. Tsou[d], G.W.M. Peters[a,b,*]

[a] Department of Mechanical Engineering, Materials Technology Institute, Eindhoven University of Technology, P.O. Box 513, 5600 MB Eindhoven, The Netherlands
[b] Dutch Polymer Institute (DPI), P.O. Box 902, 5600 AX Eindhoven, The Netherlands
[c] DSM Materials Science Center, P.O. Box 18, 6160 MD Geleen, The Netherlands
[d] ExxonMobil Chemical Company, Baytown, TX 77520, United States

ARTICLE INFO

Keywords:
Metallocene isotactic polypropylene
Flow-induced crystallization
Pressure effect
Multiphase modelling

ABSTRACT

Flow-induced crystallization at elevated pressure of a set of metallocene isotactic polypropylenes (iPP) possessing different molecular weight distributions is studied using extended dilatometry experiments in an apparatus able to apply elevated pressure (up to 1200 bar) and strong shear flow (shear rates up to 180 s^{-1}). The effect of flow on the crystallization temperature was quantified and the samples were analyzed using X-ray diffraction to measure the relative amounts of different crystal phases.

The experimental results were used to test a flow induced crystallization model framework recently developed in our group which can describe the complex crystallization behavior of iPP and includes formation of multiple morphologies (spherulites, shish-kebab structure with lamellar branching) and crystal phases (α, β and γ). Almost all model parameters were left unchanged, except for the temperature description of the quiescent crystal growth rate and nucleation density (experimentally measured using optical microscopy) and an extra parameter which takes into account the fraction of high molecular weight for the creation of flow-induced nuclei.

The model describes rather good the experimentally observed trends for what regards crystallization temperature and amount of α and γ-phase but substantial discrepancies were found in the amount of β-phase formed. This could be related to the presence of 2,1 insertion errors in metallocene samples which could inhibit the formation of this crystal phase.

1. Introduction

Isotactic polypropylene (iPP) is a remarkable and fascinating example of polymer exhibiting different crystal phases and morphologies. Its complex crystallization behavior is dependent on molecular architecture and, especially, on processing conditions: the most common monoclinic α-phase [1], is formed at ambient pressure and for low/moderate cooling rates. The β modification is usually formed using specific nucleating agents [2–4] or from oriented α-crystals created by moderately strong flow [5]. Elevated pressure and high crystallization temperatures induces the γ-phase [6,7], which is found also in iPPs with stereo- and/or regio-errors [8–10] or small amount of α-olefines comonomer [11]. Elevated cooling rates (>100 °C/s) inhibit the stable monoclinic modification in favour of a mesomorphic form [1,12]. Two other modification (δ [13] and ϵ [14]) have been reported in literature, but they are outside the scope of this work.

Processing also strongly affect the morphology of the material: fast cooling induces a peculiar not-spherulitic, nodular morphology [15] whereas elevated pressure, shifting the undercooling, causes an increase in the number of nuclei, resulting in a smaller spherulite size if compared to ambient pressure. Moderate flow conditions have the same effect while strong flow rates induce formation of fibrillar crystals called shish which can nucleate lamellae growing radially, named kebabs [16].

In the case of iPP, the shish kebab morphology possesses extra-levels of complexity: kebabs, which are usually in the stable α-phase, provide with their (0 1 0) lateral surfaces nucleation sites for additional morphologies called daughters lamellae [17–19]. These are usually in the α-modification (growing at an angle of 40°from the parents kebabs), but, when flow is combined with elevated pressure, γ-daughters

* Corresponding author at: Department of Mechanical Engineering, Materials Technology Institute, Eindhoven University of Technology, P.O. Box 513, 5600 MB Eindhoven, The Netherlands.
E-mail address: g.w.m.peters@tue.nl (G.W.M. Peters).
[1] Current address: SABIC T & I, STC Geleen, Urmonderbaan 22, P.O. Box 319, 6160 AH Geleen, The Netherlands.

http://dx.doi.org/10.1016/j.eurpolymj.2017.09.042
Received 30 May 2017; Received in revised form 5 September 2017; Accepted 25 September 2017
Available online 24 October 2017

morphologies are also found [20].

It is easy to imagine, that during real processing conditions, since the crystallizing polymer is subjected to different temperature gradients (cooling rates), complex flow fields and eventually elevated pressure, homogeneity of phases and morphologies is not an option. Exemplar is the case of iPP injection molded products, containing up to four different crystal phases (α,β,γ and mesophase) [21,22] and morphologies ranging from spherulitic (in the core), to shish-kebabs with lamellar branching (in the shear layer) to nodular (in the skin/quenched layer).

Since both structure and morphology are determining key factors for the final properties of the material [23], being able to predict them is paramount to prevent undesired morphologies or to design products with tailored properties.

The pioneering work in understanding and modelling flow-induced crystallization started by the Janeschitz-Kriegl group [24] was developed and implemented during the last twenty years in our group [25–28,19,29,30]: the temperature and pressure dependence of growth of different crystal phases and of the overall nucleation density was determined using an optimization routine to fit experimental data and described by phenomenological equations, the effect of flow on the increase in the number of nuclei and on oriented structures formation was evaluated by considering the momentary stretch of the high molecular weight tail of the material, using different approaches over the past years. The structure development in non-isothermal conditions after flow at different pressures was computed using a modified set of Schneider rate equations [31] combined with Kolmogorov-Avrami equation [32] to account for impingment.

Last and important step in this developing framework, was recently put forward by Roozemond et al. [33]: his approach combines two phenomenological models that were validated in previous works for multiphase non-isothermal structure development [27] and flow induced-crystallization with multiple morphologies (parents/daughters) [29]. New concepts were introduced, as the growth of γ-kebabs, an increased growth rate for the α-parents morphologies during and after flow and a fixed fraction of β-phase nuclei created by flow. Model results were validated on experimental data for a single Ziegler-Natta iPP over a broad range of flow conditions, temperature and pressure, showing excellent agreement.

In this work, we use the same modeling framework for predicting extended dilatometry results obtained on three iPP grades produced by metallocene catalysis, having different weight average molecular weight and unimodal and bimodal distributions. Almost all the model parameters were left unchanged, except for the temperature dependence of the quiescent crystal growth rate and nucleation density, measured using optical microscopy.

The aim of showing the universality of our modeling approach for a broader range of material characteristics and conditions is presented in the following manuscript.

2. Experimental

2.1. Materials

The materials employed for this study are a set of isotactic polypropylenes synthesized using metallocene catalysts and having different molecular weights and molecular weigth distributions. Slurry reactors were employed for the synthesis of low MW, high MW, and bimodal isotactic polypropylene (iPP) using a silica supported metallocene catalyst. A pseudo C2-symmetric rac-dimethylsilyl(4-0-biphenyl-2-n-hexylindenyl)(2-methyl-4-(3′,5′-di-tertbutyl-4′-methoxyphenyl)-indenyl) zirconium dichloride was activated with MAO (methylaluminoxane) impregnated silica particles. A single slurry reactor was used to prepare LMW and HMW iPPs using bulk propylene as the diluent running at 75 °C. The molecular weight was controlled by the amount of hydrogen used. For a bimodal iPP, two slurry reactors in series were employed where the first reactor was used to synthesize high MW iPP and the second was for low MW iPP. All iPPs thus prepared were characterized by GPC-IR (gel permeation chromatography-infrared detector) for MWD (molecular weight distribution) and by C13 NMR (nuclear magnetic resonance) for tacticity and 2,1 insertion defects.

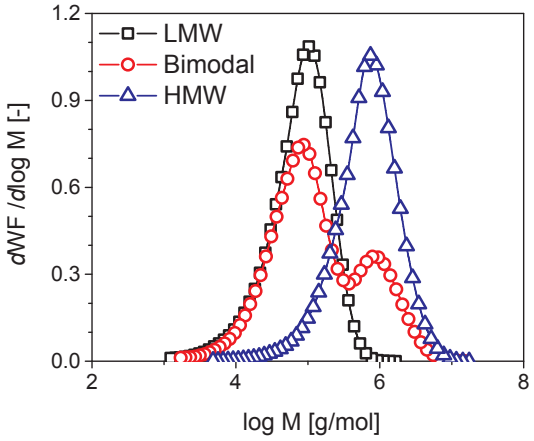

Fig. 1. GPC traces of the three materials employed in this study. The dashed lines represent fitted log-normal distributions for the bimodal material, used for determining the high and low molecular weight fractions.

Two grades, named in this work LMW and HMW, present unimodal molecular weight distributions centered at 100 and 1000 kg mol^{-1}, respectively. A third material has a bimodal distribution containing 73%$_{wt}$ of low molecular weight component (≈100 kg mol^{-1}) and 27%$_{wt}$ of high molecular weight fraction (≈1000 kg mol^{-1}) (weight percentages were calculated fitting Log-normal distribution to the molecular weight distribution obtained from GPC measurements). Molecular weight distributions obtained from GPC-IR measurements and related molecular weight parameters are presented in Fig. 1 and in Table 1 together with the percentage of [mmmm] pentad and the regio defects.

To prevent degradation and chain scission during processing at elevated temperature, the following amounts of stabilizers were added to all the materials using a DSM MC 15 micro compounder: 1500 ppm Irganox 1010, 1500 ppm Irgafos 168, 500 ppm DHT-4 V, and 150 ppm Irganox E201 (Vitamin E).

2.2. Extended dilatometry

Experiments were performed in the Pirouette extended dilatometer (IME Technologies), which has been employed in several works performed in our group during the last years (see References [34,35,28,30]). This apparatus is able to monitor the specific volume of a material in a broad range of temperature (T = 25–300 °C) and pressure (p = 1–1200 bar) and it possesses the exceptional ability to apply shear flow in a Couette cell ($\dot{\gamma}$ = 1–180 s^{-1}) to the molten polymer.

The ring-shaped PVT samples have a mass of ≈75 mg with dimensions 22 × 21 × 2.5 mm (outer diameter × inner diameter × height), and are produced using a Babyplast mini-injection molding machine.

The experimental protocol consists of the following steps: first, the sample is heated to 250 °C and kept at this temperature for 5 min to

Table 1
Characteristics of the three iPPs samples obtained from GPC-IR and C13 NMR. Regio defects refers to 2,1 insertion errors.

Material	M_n [kg mol^{-1}]	M_w [kg mol^{-1}]	M_z [kg mol^{-1}]	M_w/M_n [–]	[mmmm] [%]	Regio defects [%]
LMW	40	112	198	2.80	0.958	0.54
Bimodal	51	420	1’787	8.24	0.968	0.59
HMW	337	1’000	2’061	2.97	0.967	0.61

Table 2
Overview of all experimental conditions used in this work.

Pressure p (bar)	Undercooling $\Delta T_{\dot{\gamma}}$ (°C)	Shear temperature $T_{\dot{\gamma}}$ (°C)	Shear rates $\dot{\gamma}$ (s^{-1})
100	30	168.2	0, 10, 30, 100, 180
500	30	180	0, 10, 30, 100, 180
900	30	192	0, 10, 30, 100, 180
1200	30	201	0, 10, 30, 100, 180

erase any previous thermo-mechanical history, it is then pressurized to the desired pressure (100, 500, 900 and 1200 bar) and cooled down to room temperature with an average cooling rate of ≈1 °C/s. During cooling, the material is subjected to shear flow for 1 s using different shear rates ($\dot{\gamma}$ = 0, 3, 10, 30, 100, 180 s^{-1}) at a fixed undercooling ($\Delta T_{\dot{\gamma}}$) of 30 °C. The undercooling ($\Delta T_{\dot{\gamma}} = T_m^{0,p} - T_{\dot{\gamma}}$) is defined as the difference between the equilibrium melting temperature, T_m = 195 °C for iPP [36], and the shear temperature, $T_{\dot{\gamma}}$. The dependence of the melting temperature from the pressure was taken in account according to the well known Clapeyron equation [37]:

$$T_m^{0,p} = T_m^{0,p_0} + \zeta(p - p_0), \quad (1)$$

where p is the pressure at which the experiment is conducted, p_0 = 1 bar the reference pressure pressure and ζ a thermodynamic constant for the pressure dependence of the melting temperature, taken to be 30 °C $kbar^{-1}$ [38]. An overview of the experimental conditions used is given in Table 2.

The absolute specific volume temperature evolutions obtained from dilatometry experiments are converted to a normalized specific volume (ν^*), to compare experiments performed at different thermo-mechanical histories (different pressures and shear rates), using:

$$\nu^* = \frac{\nu - \nu_s}{\nu_m - \nu_s}, \quad (2)$$

where ν is the measured specific volume, ν_s the value of specific volume in the solid state at 40 °C, and ν_m the value of specific volume in the melt at 220 °C.

The normalized specific volume is used to determine the experimental onset of the crystallization temperature (T_c), defined as the intersection of the slopes fitted on the specific volume evolutions in the melt state and during solidification, as shown in Fig. 2. According to this procedure, T_c corresponds to a total space filling of ≈10%. The effect of flow on the crystallization kinetics is quantified using the dimensionless crystallization temperature θ, defined as:

$$\theta = \frac{T_c^{\dot{\gamma}}}{T_c^{Q}}, \quad (3)$$

where $T_c^{\dot{\gamma}}$ and T_c^{Q} are the crystallization temperatures with and without an applied shear flow, respectively.

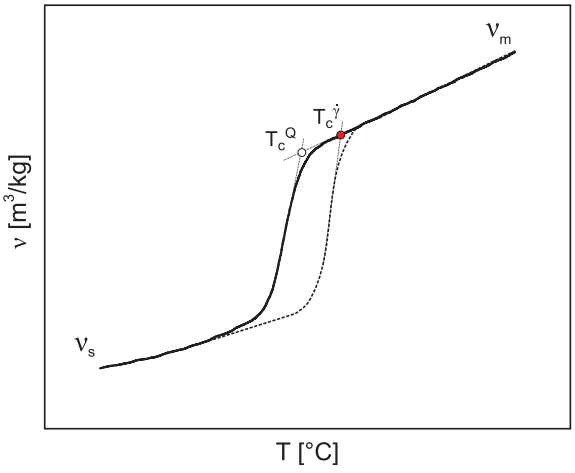

Fig. 2. Schematic of the experimental analysis protocol applied to PVT measurements. Solid line: crystallization under quiescent conditions, dashed line: crystallization after shear pulse. Adapted from van Erp [28].

2.3. Wide angle X-ray diffraction

Wide angle X-ray diffraction (WAXD) measurements were performed using a Bruker D8 Discover equipped with a GADDS 2D detector and using Ni-filtered Cu-K_α radiation (λ = 1.54 Å). WAXD two-dimensional images were acquired in transmission (in the direction perpendicular to flow in the Couette cell) for 480 s at a distance of 100 mm from the sample and corrected for the scattering of the air background. 2D images were reduced to 1D intensity vs 2θ profiles and an amorphous halo, obtained from the X-ray diffraction profile of an atactic polypropylene, was scaled and subtracted from the diffraction profiles of each sample.

The contribution to the diffraction due to the different crystal phases was analysed according to a deconvolution procedure similar to the one proposed by Turner-Jones [39]: 7 pseudo-Voigt fuctions were used to fit the diffraction peaks, and the area underneath $(130)_\alpha$ ($A_{(130)_\alpha}$) and the $(117)_\gamma$ ($A_{(117)_\gamma}$) were taken as a measure of the amount of the α and γ polymorphs, respectively.

The fraction of the two phase was then evaluated using:: $f_\gamma = A_{(117)_\gamma}/[A_{(130)_\alpha} + A_{(117)_\gamma}]$ and $f_\alpha = A_{(130)_\alpha}/[A_{(130)_\alpha} + A_{(117)_\gamma}]$.

2.4. Rheology

Determining factor for our modelling approach is the quantification of the rheology of the material: the rate of formation of nuclei due to flow and the longitudinal growth of shish structure is calculated from the polymer backbone stretch on a continuum level using the extended Pom-Pom (XPP) constitutive model [40].

Since it is widely recognized that it is the high molecular weight tail of the material to be crucial for flow-induced crystallization [41–47], only the longest mode (related to the HMW tail) is taken as representative in calculating the molecular stretch as follows:

$$\overset{\nabla}{\mathbf{c}} + 2\frac{\exp[\nu(\sqrt{\mathrm{tr}\mathbf{c}/3} - 1)]}{\tau_R^{HMW}}\left(1 - \frac{3}{\mathrm{tr}\mathbf{c}}\right)\mathbf{c} + \frac{1}{\tau_o^{HMW}}\left(\frac{3\mathbf{c}}{\mathrm{tr}\mathbf{c}} - \mathbf{I}\right) = 0, \qquad \Lambda_{HMW} = \sqrt{\mathrm{tr}(\mathbf{c}/3)}. \quad (4)$$

In which $\overset{\nabla}{\mathbf{c}}$ is upper convected derivative the conformation tensor ($\mathbf{c}$), q the number of arms and ν given by $\nu = 0.1/q$,τ_o^{HMW} and τ_R^{HMW} the orientation relaxation (reptation) time and the stretch-relaxation (Rouse) time of the high molecular weight fraction of the material, respectively.

Orientation relaxation times for the three material were extracted from small amplitude oscillatory shear measurements. The characteristic rheological properties (storage and loss modulus, G′ and G″) were obtained over a broad range of temperatures (from 150 to 230 °C) and angular frequencies ω (from 0.01 to 100 rad s^{-1}). Time-temperature superposition was applied to obtain mastercurves at a reference temperature of 190 °C. The temperature shift factors (a_T) were calculated using a WLF-description:

$$\log(a_T) = -\frac{c_1(T - T_{ref})}{c_2 + (T - T_{ref})}, \quad (5)$$

where T_{ref} is the reference temperature (190 °C), and c_1 and c_2 the WLF constants.

The relaxation time spectrum is calculated from the mastercurves by fitting a discrete Maxwell relaxation time spectrum (g_i,τ_i) and the longest relaxation time from the discrete spectrum of each material was

taken to be the orientation relaxation time in the XPP model.

The stretch relaxation times (τ_R, necessary to calculate backbone stretch in the XPP model) are more difficult to determine, as the materials show very little strain hardening in the range of strain rates that can be measured using extensional rheology. Therefore, we use a scaling argument based on the Doi-Edwards theory [48]: the stretch-relaxation time (also called Rouse time) scales with the square of the molecular weight: $\tau_R \propto M_w^2$.

The material used in references [28,29,33] has a molecular weight of 365 kg mol^{-1} and the longest stretch relaxation time is 3.7 s at 190 °C. Consequently, we assume the stretch relaxation time of the LMW material (M_w = 100 kg mol^{-1}) and of the HMW (M_w = 1000 kg mol^{-1}) to be 0.25 and 25 s, respectively. Since the bimodal material possesses an high molecular weight distribution centered at 1000 kg mol^{-1}, its Rouse time is considered to be the same as the HMW material. For the parameter q (number of arms) the same value as Roozemond is assumed for all materials (q = 12). The scaling approach for evaluating the stretch relaxation times could appear quite casual, since the effect of polydispersity is neglected (the metallocene iPPs subject of study have a narrower polydispersity if compared to the ZN iPP used in references [28,29,33]) and the number of arms q is kept constant, whereas it should be a fitting parameter for the extensional rheology data.

Nevertheless, our aim is to show the universality of our crystallization model for iPP, and all the parameters for the flow induced nucleation described in Section 3.3 are tuned accordingly to the rheological ones, as determined by van Erp and Roozemond [28,29,33]. To our opinion, the scaling argument for the stretch relaxation times and the assumption of a constant value of the q paramenter would be the best way, also for a future third party, to use this model without varying too many parameters. Using this approach, no difficult fitting of extensional rheology data would be needed, and only orientation relaxation times obtained from small amplitude oscillatory shear measurements are required.

All rheological parameters are presented together with the WLF constants in Table 3 for each material. When solving the molecular stretch at different pressure, the pressure shift factor was used according to [49,50]:

$$a_p = \exp(\kappa(p - p_{ref})), \tag{6}$$

where κ = 16.18 GPa^{-1} and p_{ref} = 1 bar the reference pressure.

2.5. Polarized optical microscopy

The nucleation density and the crystal growth rate of the α-phase for the different materials were determined by polarized optical microscopy experiments. A thin slice of material was heated up to 230 °C in a Linkam hot stage for 5 min to erase any previous thermo-mechanical history and subsequently cooled down to different isothermal crystallization temperature with a cooling rate of 30 °C/min. Once the isothermal crystallization temperature was reached, images were acquired over time to determine the overall growth rate by measuring the time evolutions of the radii of several growing spherulites. Since microscopy experiments were conducted at ambient pressure and in a temperature range (130–160 °C) only favourable to the formation of α-phase crystals, the linear fit shown in Fig. 3 was used to obtain the α-crystal growth rate at each temperature. Once spherulites reached impingement (space filling was complete), the number per micrograph, N_A, was counted in the visible field, at different positions within the sample. Knowing the observed area, A_{mic}, the approximate nucleation density per unit volume was evaluated according to Janeschitz-Kriegl et al. [51,52]:

$$N = \left(\frac{N_A}{A_{mic}}\right)^{3/2}. \tag{7}$$

The analyzed microtomy area was about 0.5 mm^2, and at least 2 or 3 different micrographs were employed per crystallization temperature.

Table 3
WLF constants and orientation relaxations times for the different materials at T_{ref} = 190 °C.

Material	c_1 [°C^{-1}]	c_2 [–]	τ_0 [s]	τ_R [s]	q [–]
LMW	3.2529	318.6857	0.525	0.25	12
Bimodal	0.5910	60.9154	580	25	12
HMW	3.2386	341.8496	580	25	12

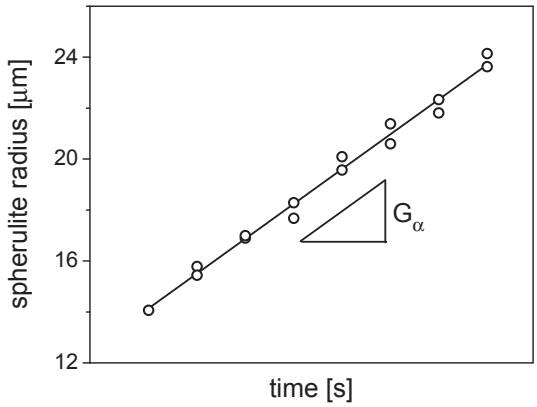

Fig. 3. Time evolution of the spherulites' radii for the HMW material obtained from microscopy experiments at 151 °C. The line represents the linear fit employed to calculate the linear growth rate of α-phase.

3. Crystallization model framework

Flow-induced crystallization of isotactic polypropylene at elevated pressure in multiple phases and multiple morphologies is described in this work according to the latest version of the modelling framework recently implemented in our group by Roozemond et al. [33]. This framework was formulated by combining the concept presented by van Drongelen [27] for the influence of pressure and temperature on the quiescent crystallization of iPP different crystal phases (α,β and γ) and including the effect of flow on point- (spherulites) and line-nucleation (shish) kinetics, as firstly proposed by van Erp [28] and lately extended by Roozemond [29].

Crystal nuclei are created by cooling down or by application of flow, and are assigned to a certain crystal phase according to a weight factor based on their momentary growth rates. Each nucleus grows with its respective crystal phase growth rate, dependent on pressure and temperature, until unitary space filling is reached (impingement). Mathematically, this is translated by a set of modified Schneider rate equations [53], which are solved to calculate the overall crystallization kinetics of spherulites in multiple phases and shish-kebab with α and γ-phase lamellar branching.

The temperature dependence of both nucleation density and crystal growth rates, is key for this work, since the parameters used in references [27,33] were optimized on a very well characterized Ziegler-Natta iPP grade, whereas the polymers object of this work are synthesized by metallocene catalysis and present different molecular weight distributions.

Since we want to show the universality of our modelling approach, we try to keep the same as many parameters as possible, and we will carefully tune only those which permit a more accurate description of the data obtained from optical microscopy experiments.

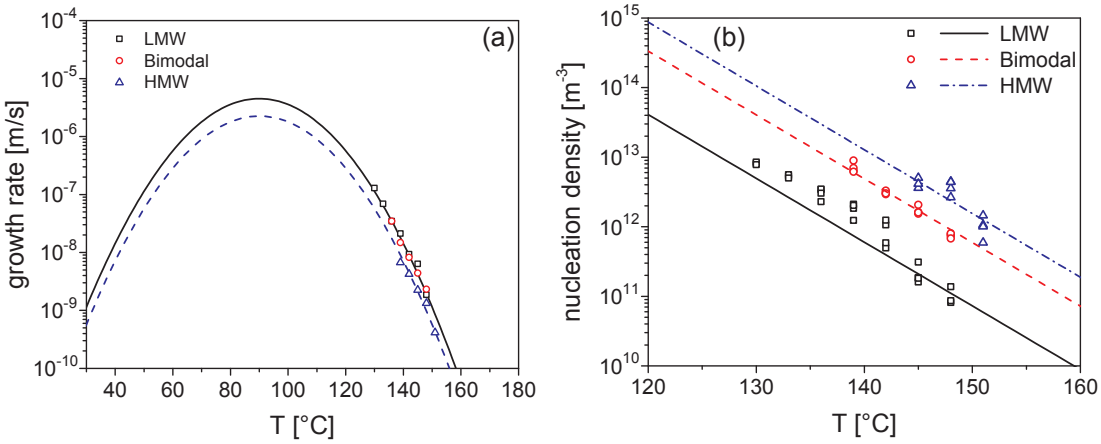

Fig. 4. (a) α-crystal growth rate and (b) quiescent nucleation density. Markers are values extracted from microscopy experiments and lines are α-crystal growth rates (a) and quiescent nucleation density (b) for the three different materials according to Eqs. (8) and (11), respectively.

3.1. Crystal growth rate

The linear growth rates of α-phase spherulites for the three different materials measured from POM experiments are shown as open markers in Fig. 4a. Two main observations can be extracted from the experimental results: the growth rates of the LMW material are practically the same as the bimodal, whereas the HMW grade shows slightly slower growth in the investigated temperature range. The influence of molecular weight on the maximum growth rates has been investigated in literature [54–56], and a decrease with increasing molecular weight is expected, in line with our experimental observations.

In this work we use an empirical relation to describe the growth rate of each crystal phase (α,β and γ), which, similarly to the widely used Lauritzen-Hoffman theory [57], translates to a bell-shaped curve to describe the temperature dependence of the growth rate:

$$G_i(T) = G_{\max,i}\exp(-c_{G,i}(T-T_{\mathrm{Gref},i})^2), \tag{8}$$

where G_i is the crystal growth rate of a specific phase, $G_{\max,i}$ the growth rate at the reference temperature $T_{\mathrm{Gref},i}$ and c_G a constant parameter describing the temperature dependence of the growth rate. Subscript $i$denotes the possible different phases.

The shift of the reference temperature of all phases with pressure is tuned using the Clapeyron equation (Eq. (1)). Pressure also increases the maximum growth rate of the γ-phase according to an exponential relation:

$$G_{\max,\gamma} = G_{\max,0,\gamma}\exp(\alpha_\gamma(p-p_0)), \tag{9}$$

with $\alpha_\gamma = 7.7\cdot10^{-4}$ and $p_0 = 1$ bar, the reference pressure.

Both the α-growth rate of the LMW and bimodal material can be accurately captured by Eq. (8) using the parameters employed in references [27,33] (see full line Fig. 4a).

The decrease of the maximum in growth rate for the high molecular weight material is taken into account decreasing solely the value of $G_{\max,\alpha}$ (of a factor 2) to fit the experimental data. Consequently, the decrease of $G_{\max}$ for the other crystal phases (β and γ) is assumed to be proportional to the decrease $G_{\max,\alpha}$.

The parameters used for the growth rate functions of the three crystal phases are summarized in Table 4. The good agreement between the set of parameters and the experimental data is shown in Fig. 4a where the lines represent the growth rate for the α-phase evaluated using Eq. (8) for the three different materials.

Finally, the growth rate of the α-phase nucleating directly from the shish backbone (so called α-parents lamellae) is enhanced by flow, since this lamellae present their chain axes oriented in the direction of flow [29,17]. The increase in α-growth rate persist also immediately when flow is stopped, and relaxes back to the quiescent value when the chain orientation is lost. In our formulation there is not direct dependence from the momentary molecular stretch or orientation but the effect is taken into consideration by using an empirical relation which showed good agreement with the experimental data in reference [29]:

$$G_{\alpha,\mathrm{p}}(T,t) = G_\alpha(T)(1 + G_{\mathrm{flow}}\exp(-t/\lambda_G)), \tag{10}$$

with $G_{\alpha,\mathrm{p}}$ the growth rate of the α-parents morphology, $G_{\mathrm{flow}} = 4$ and $\lambda_G = 9$ s empirical parameters.

Table 4
Parameters for crystal growth rate for the three different materials used.

Growth rate	LMW Bimodal			HMW		
	α	β	γ	α	β	γ
$c_{G,i}$ [10^{-3} °C^{-1}]	2.3	6.6	3.5	2.3	6.6	3.5
$T_{\mathrm{Gref},i}$ [°C]	90	107	104	90	107	104
$G_{\max,i}$ [μm s^{-1}]	4.8	7.1	1.1	2.4	3.55	0.55

3.2. Nucleation density

Fundamental for our modeling framework is to quantify the temperature dependence of the quiescent nucleation density since, this is strongly dependent on the impurities and additives present in the polymer, it can vary from one material to another.

The three iPPs show different values of the nucleation densities but a similar temperature dependence (same exponential decay). The HMW material shows the highest values of the nucleation density, followed by the bimodal and the LMW. Since the same amount of support catalyst particles and the same amount of additives was used during the preparation and the processing of the three materials, one could expect the nucleation density be similar among the three. A plausible explanation would be that, since the materials were processed using extrusion (for blending the additives) and injection molding (for preparing the PVT samples) which involve high deformation and shear rates of the polymer melt, some flow induced-nuclei could remain in the high molecular weight material also after annealing at 230 °C for 10 min causing a self-seeding effect which leads to higher nucleation densities for the HMW and the bimodal [45,58].

Based on this observation, we describe the temperature dependency of the quiescent nucleation densities, used in our model, by mean of an empirical relation as in Ref. [27,28,33]:

$$N_q(T) = N_{\mathrm{ref}}\exp(-c_N(T-T_{\mathrm{N,ref}})), \tag{11}$$

where 145 °C is selected as reference temperature ($T_{\mathrm{N,ref}}$) and N_{ref} is the experimentally measured nucleation density at this temperature

Table 5
Parameters for quiescent nucleation for the three different materials used.

Nucleation density	LMW	Bimodal	HMW
c_N [°C^{-1}]	0.211	0.211	0.211
$T_{N,ref}$ [°C]	145	145	145
N_{ref} [m^{-3}]	$2.09 \cdot 10^{11}$	$1.71 \cdot 10^{12}$	$4.46 \cdot 10^{12}$

(obtained from the average of different values measured using microscopy). The factor c_N, which describes the slope of the decay, is assumed to be the same as in reference [33], since it provides a reasonably good description of the experimental data (See Fig. 4a). An overview of the parameters used is given in Table 5.

Upon cooling, the quiescent nucleation rate is simply given by:

$$\dot{N}_q = \dot{T}\frac{dN_q}{dT}. \tag{12}$$

3.3. Flow-induced nucleation and longitudinal shish growth

As already stated earlier in this work, the creation of nuclei due to flow is related to stretch of polymer chains constituting the high molecular weight fraction of the molecular weight distribution.

Therefore, the formation rate of new nuclei due to flow ($\dot{N}_f$) is coupled, in a phenomenological manner, with the momentary stretch (Λ_{HMW}) of the HMW tail on a continuum level evaluated using Eq. (4). The equation reads:

$$\dot{N}_f = g_n(T,p)\exp(\mu_n(\Lambda_{HMW}^2 - 1)), \tag{13}$$

with μ_n and g_n scaling parameters determined in reference [33]. The effect of pressure and temperature on the flow nucleation rate is included in the momentary stretch (relaxation times shift with T and p) and in the parameter g_n as follow:

$$g_n(T,p) = \phi_{hmw} g_{n,ref}\, 10^{c_{n,T}(T-T_{ref})+c_{n,p}(p-p_{ref})}, \tag{14}$$

with $g_{n,ref}$, $c_{n,T}$ and $c_{n,p}$ parameters determined by Roozemond [33].

Since the bimodal and the HMW material have the same high molecular weight component, the rheology for the longest mode is identical (see Table 3). We need to take into account the different concentration of HMW chains (responsible of flow induced nucleation) using the additional parameter ϕ_{hmw}: this represent the fraction of chains representative of the longest relaxation modes (those with high molecular weight). It easily follows that $\phi_{hmw} = 1$ for the HMW material and $\phi_{hmw} = 0.27$ for the bimodal (as determined from GPC, see Section 2.1).

In case of strong flow conditions, highly oriented fibrillar crystals (shish), able to nucleate lamellae in the α and γ-phase, are formed. Their longitudinal growth is related to flow induced nucleation using a formulation inspired by the "streamers" concept introduced by Kornfield and co-workers [59]: shish propagation starts from flow-induced nuclei and is driven by addition of chain segments to the tip of the developing shish during flow. Assuming affine deformation (due to the high local deformation rates), the longitudinal propagation rate is defined:

$$\dot{L}_{tot} = 2N_f \dot{\gamma} \xi_{seg}, \tag{15}$$

where $\dot{\gamma}$ is the shear rate and $\xi_{seg} = 5$ nm.

Overview of the parameters for flow-induced nucleation and shish longitudinal development is given in Table 6.

The overall nucleation rate is the sum of the nucleation rate due to cooling ($\dot{N}_q$) and to flow ($\dot{N}_f$). The nuclei reservoir is assigned to the different phase according to a weight factor (f_i):

$$\dot{N}_i = f_{i,q}\dot{N}_q + f_{i,f}\dot{N}_f, \tag{16}$$

where $f_{i,q}$ and $f_{i,f}$ are the factors for quiescent and flow induced nucleation rates.

Table 6
Parameters for flow-induced nucleation at T_{ref} = 166 °C and p_{ref} = 100 bar.

Parameter	Value
μ_N [–]	0.03
ϕ_{hmw} [–]	1 (HMW, LMW) 0.27 (Bimodal)
$g_{n,ref}$ [m^{-3}s^{-1}]	10^{12}
$c_{n,T}$ [°C^{-1}]	−0.016
$c_{n,p}$ [bar^{-1}]	$7.58 \cdot 10^{-4}$
ξ_{seg} [nm]	5

In quiescent conditions, no β-phase is formed and the nuclei are assigned to the α or to the γ phase according to their momentary growth rates ($f_{\alpha,q} = G_\alpha/G_\alpha + G_\gamma$ and $f_{\gamma,q} = G_\gamma/G_\alpha + G_\gamma$).

When flow is applied, the model assumes the formation a fixed fraction of β nuclei ($f_\beta = 0.002$, 2%), this nuclei are subtracted to the overall reservoir and can only grow in β-phase spherulites.

The weight factors for flow induced nuclei are then defined as:

$$\begin{aligned} f_{\alpha,f} &= (1-f_{\beta,f})\frac{G_\alpha}{G_\alpha + G_\gamma}, \\ f_{\beta,f} &= 0.002, \\ f_{\gamma,f} &= (1-f_{\beta,f})\frac{G_\gamma}{G_\alpha + G_\gamma}. \end{aligned} \tag{17}$$

3.4. Schneider rate equations

Crystallization kinetics of spherulites and shish kebab with parents-daughters morphology were evaluated using an extended and modified version of Schneider rate equations [31].

In our modelling approach, point nuclei are created upon cooling or by application of flow: at the moment of their formation, they are assigned to each phase using a weight factor based on their momentary growth rate.

Kinetics of formation of shish-kebabs structure with multiple morphology is a more complicated story: after shish are created during flow, both α and γ-kebabs can develop (both denoted as parent morphologies) from their backbone. From the α-parents lamellae, lamellae in daughters morphology, both in α and γ-phase grow with an angle of 40°and 80°, respectively. Differently, γ-kebab can only nucleate γ-daughters.

The relative fraction of each morphology is, again, proportional to the momentary growth rate of the different phases (and morphology). Only the α-parents morphology, possessing chain axes in the direction of flow, has an increased growth rate during a certain time scale, as stated in Eq. (10). The growth of all the other morphology is assumed to be proportional to the quiescent growth rate of each phase.

All these concepts are mathematically translated in the set of differential equation presented in Table 7.

Finally, the correction for the impingement of the different morphologies is introduced by the Kolmogorov-Avrami equation [32]:

$$\xi_{tot} = 1 - \exp(-\sum \phi_{0,i} + \psi_{0,i}), \tag{18}$$

where ξ_{tot} is the total space filling, equal to 1 at the end of crystallization. For each phase i, the individual space filling easily follows: $\dot{\xi}_i = (1-\xi_{tot})(\dot{\phi}_{0,i} + \dot{\psi}_{0,i})$.

4. Results

As stated before, aim of this paper is to demonstrate the applicability of the latest version of our crystallization model framework, applied so far to a single Ziegler-Natta iPP, to a set of materials with different molecular weight distributions and synthesized using metallocene catalysts.

Table 7
Schneider rate equations used to evaluate the kinetics of all the different morphologies.

Spherulites	
$\dot{\phi}_{3,i} = 8\pi\dot{N}_i$	($\phi_3 = 8\pi N$, number)
$\dot{\phi}_{2,i} = G_i\phi_{3,i}$	($\phi_2 = 8\pi R_{tot}$, radius)
$\dot{\phi}_{1,i} = G_i\phi_{2,i}$	($\phi_1 = S_{tot}$, surface)
$\dot{\phi}_{0,i} = G_i\phi_{1,i}$	($\phi_0 = V_{tot}$, volume)
Shish-kebabs	
$\dot{\psi}_{1,\alpha} = 4\pi G_\alpha L_{tot}\frac{G_\alpha}{G_\alpha + G_\gamma}$	(surface α-parents)
$\dot{\psi}_{1,\gamma} = 4\pi G_\gamma L_{tot}\frac{G_\gamma}{G_\alpha + G_\gamma}$	(surface γ-parents)
$\dot{\psi}_{0,\alpha,p} = G_{\alpha,p}\psi_{1,\alpha}\frac{G_{\alpha,p}}{G_{\alpha,p} + G_{\alpha,d} + G_\gamma}$	(volume α-parents)
$\dot{\psi}_{0,\alpha,d} = G_{\alpha,d}\psi_{1,\alpha}\frac{G_{\alpha,d}}{G_{\alpha,p} + G_{\alpha,d} + G_\gamma}$	(volume α-daughters)
$\dot{\psi}_{0,\gamma,p} = G_\gamma\psi_{1,\gamma}$	(volume γ-parents)
$\dot{\psi}_{0,\gamma,d} = G_\gamma\psi_{1,\alpha}\frac{G_\gamma}{G_{\alpha,p} + G_{\alpha,d} + G_\gamma}$	(volume γ-daughters)

Only two paramenters in the temperature dependence of the growth rate and nucleation density were modified to better describe the experimentally measured values (N_{ref} for each individual material and G_{max} only for the HMW).

Moreover an additional parameter (ϕ_{hmw}) was introduced to describe the flow induced nucleation rate for the bimodal material: this was necessary because, in the previous formulation, the concentration of chains representative of the longest relaxation modes, responsible of the flow-induced nucleation/crystallization, was not explicitly taken into account.

Throughout this manuscript, the experimental results from dilatometry will be compared to the output from the multi-phase multi-morphological crystallization model, commenting agreement and discrepancies, and suggesting the possible causes for the latter.

4.1. Dimensionless crystallization temperature

The dimensionless crystallization temperatures obtained from dilatometry experiments (θ, evaluated according to Eq. (3)) as a function of the shear rate corrected for the pressure and temperature at with shear flow is applied are plotted in Fig. 5 together with the model predictions for the three materials object of this study.

As expected for materials possessing different molecular weight distributions, the effect of flow on the experimental crystallization temperature varies greatly.

Flow has hardly any influence on the crystallization of the LMW iPP, and only the experiments performed using a shear rate of 180 s^{-1} at all pressures (100, 500, 900, 1200 bar) show a small shift from the quiescent crystallization temperature values (see Fig. 5a). For the bimodal material (Fig. 5b), a relatively mild increase of the crystallization temperature is observed above a certain value of the shear rate whereas the HMW material, as clear from Fig. 5c, shows 2 regimes beyond the one where flow has no effect (at low shear rates): a moderate increase of the crystallization temperature already at relatively low shear rates (values of $a_T a_P\dot{\gamma}$ lower than 100 s^{-1}) and a substantial increase of θ for strong flow rates (values of $a_T a_P\dot{\gamma} \gg 100$ s^{-1}).

These different regimes for the increase dimensionless crystallization temperature were defined by Van Erp et al. in previous work [35,28] performed using the same experimental setup. Regime I is defined in the range of shear rates where flow has no effect on the crystallization temperature (no deviation from the quiescent T_c value is observed), Regime II includes the experiments in which an increase in the crystallization temperature is observed but no orientation is present in the WAXD profiles, indicating an increase in point-nucleation. Finally, Regime III includes the experiments in which oriented crystals are formed, resulting in a big increase of the crystallization temperature if compared to the quiescent case.

Clearly, only the experiments conducted on the HMW material show all the three different regimes, whereas the LMW and the bimodal only present flow-induced point nucleation at high shear rates.

The output from the model for the three different materials is shown as full markers in Figs. 5a, b and c: the model predicts reasonably well the general experimental trends but some deviations from the PVT data can be observed.

First, the model does not predict the onset of flow induced nucleation for the LMW material (Fig. 5a) and underestimates the crystallization temperatures in the flow induced nucleation regime for the HMW material. This disagreements between experiments and model are related to an underestimation of the stretch relaxation times used which leads to a lower number of flow induced nuclei in respect to the experimental case. We remind the reader that the Rouse times used to calculate the stretch of the high molecular weight tail of the material, according to Eq. (4), were not evaluated from fitting experimental data, but estimated from the Rouse time used by Roozemond [29,33] (for a Ziegler-Natta iPP) and using scaling arguments based on reptation theory and weight average molecular weights (see Section 2.4). The material used in Roozemond work has a broader molecular weight distribution (polydispersity index PDI ≃ 5.4) if compared to the LMW and HMW metallocene iPPs used in this work (PDI ≃ 3): deviations (underestimation of the actual Rouse times) can be expected.

Although these deviations are present, the three crystallization regimes and their onsets are well predicted for both the bimodal and the HMW material and the crystallization temperatures in Regime III (formation of oriented crystal structures) for the HMW is captured quite accurately. This is even more relevant if considered that, in the current work, all the parameters related to flow-induced nucleation and longitudinal shish growth are left unchanged with respect to the original model formulation [33] and considering the assumptions made to evaluate the stretch relaxation times (see Section 2.4).

4.2. α and γ-phases content

One of the most relevant results of our modelling multi-phase multi-morphology approach was the prediction of the relative amounts of the two predominant polymorphs, α and γ-phase. Two fundamental concepts were introduced by Roozemond et al. in a consecutive series of works [19,29,33]: α-parents lamellae (kebabs) possess an increased growth rate during flow and for a specific time after its cessation and γ-phase grows in shish-kebab structures not only from the daughter morphology (α-parents), but can also nucleate directly from the shish backbones (forming so called γ-kebabs or γ-parents morphology).

In this section, the validity of the approach and, especially, of the concept is tested, presenting side by side the volume fractions of the different phases as a function of the crystallization temperature as obtained from the experimental results and from the model predictions.

The experimentally measured α-phase volume fractions for the three different material are presented in Fig. 6a, c and e (LMW, bimodal and HMW, respectively), dashed lines are added as guides to the eye.

Similarly to van Erp [35], a decrease of the α phase fraction is observed at high crystallization temperatures and high pressure for both the LMW and the bimodal materials. This is easily ascribed to the fact that, for crystallization at low temperatures (as expected for experiments conducted at lower pressures and with no big effect of flow), the growth rate of the α-phase is clearly higher, while at high temperature and high pressure the growth of the γ-phase becomes predominant. This is even more clear if we consider the corresponding experimental γ-phase volume fraction presented in Fig. 7a and c for the LMW and the bimodal materials: the decrease in α-phase content correspond to a consequential increase in the amount of γ-phase. The effect is captured rather well by the crystallization model as evident from the model predictions for the α and γ-phase volume fraction of the LMW and the bimodal presented in Fig. 6b and d and Fig. 7b and d.

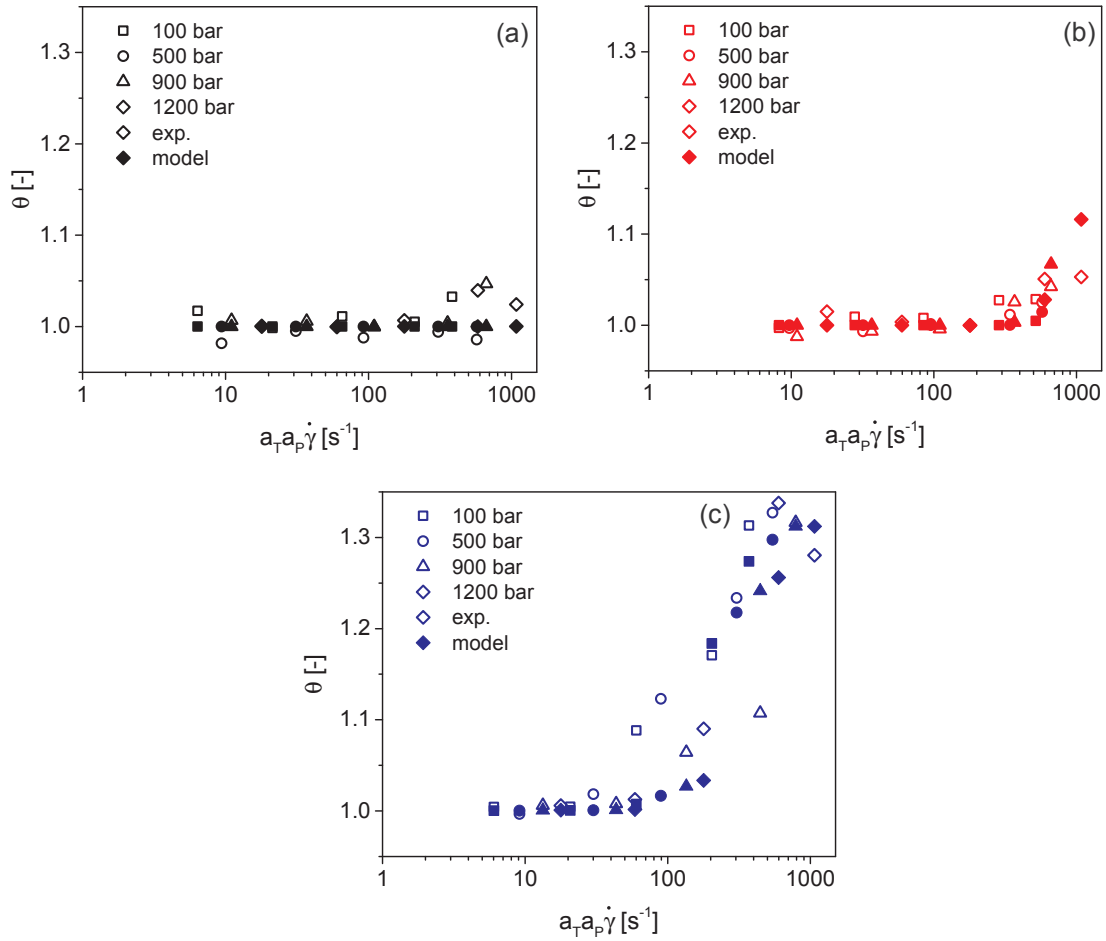

Fig. 5. Dimensionless crystallization temperature (θ) as a function of the flow strength for the LMW (a), bimodal (b) and HMW (c) materials. The open and filled markers represent experimental data and model predictions, respectively.

The experimentally observed trend of the different phase fractions as a function of the crystallization temperature for the HMW material shows instead a completely different behavior (see Figs. 6e and 7e). For the experiments where formation of oriented crystals (shish-kebab morphologies) is observed, substantial amounts of α-phase (up to 60%) are found at high temperature (up to 195 °C).

This is in agreement with the idea of an increased growth rate of the α-parents morphology during and immediately after flow, due to the fact that the α-kebab present their chain axes in the direction of flow. The concept is incorporated in the crystallization model by mean of Eq. (10) and leads to a quite accurate prediction of the α and γ-phase contents for the HMW material in the high temperature range, as evident from Figs. 6f and 7f.

Some discepancies are found at very high temperatures where the model overestimates the amount of α-phase formed (90% vs ≈65% of the experiments). Although the differences for these points are substantial, we need to remind the reader that the parameters used in Eq. (10) (G_{flow} and λ_G) were obtained from a set of experiments on a completely different material (Ziegler-Natta, different molecular weight distribution) and, moreover, we use the same growth rate function for the γ phase as used in references [27,33] for the low molecular weight and the bimodal materials (the growth rate of the γ phase was evaluated in reference [27] using in situ X-ray experiments, which unfortunately were not possible for the current study). For the HMW material, we decrease the value of the maximum in growth rate of the γ phase of a factor 2 since experimentally the same decrease is measured in the growth rate of the α phase.

This is quite a crude assumption, since the material object of study in references [27,33] had many less regio-defects than the metallocenes investigated in the current work. It is well known that the γ-form is able to host more defects in its crystal structure (see Refs. [8,9]), therefore its growth for the iPPs object of this study, is expected to be favoured over the typically stable α-form, especially in the high temperature range. Therefore, the under estimation of the amount of γ-form could be related to the aforementioned underestimation of the crystal growth rate of the γ-form, and only experimental data collected for metallocene iPPs could solve the issue in the future.

Overall, the model describes rather well the experimentally observed trends, and probably further improvements could be achieved by introducing some dependence on the molecular orientation and/or stretch for the increased growth rates of the α-parents morphology.

4.3. β-phase content

The biggest discrepancies between the experimental results and the model predictions concern the amount of β-phase formed.

In the model formulation a fixed amount of β-phase nuclei are formed upon application of flow (0.2% of the total amount of flow-induced nuclei) and can grow into spherulites as already explained in Section 3.

Although this number is extremely low, relevant amounts of β-phase can be found in samples crystallizing in the temperature range in which the crystal growth rate of the β polymorph is significantly higher (between 90 and 130 °C at ambient pressure, according to the model).

As expected, the crystallization model predicts volume fractions of β crystals as high as 20% also in our case, as evident from the analysis of

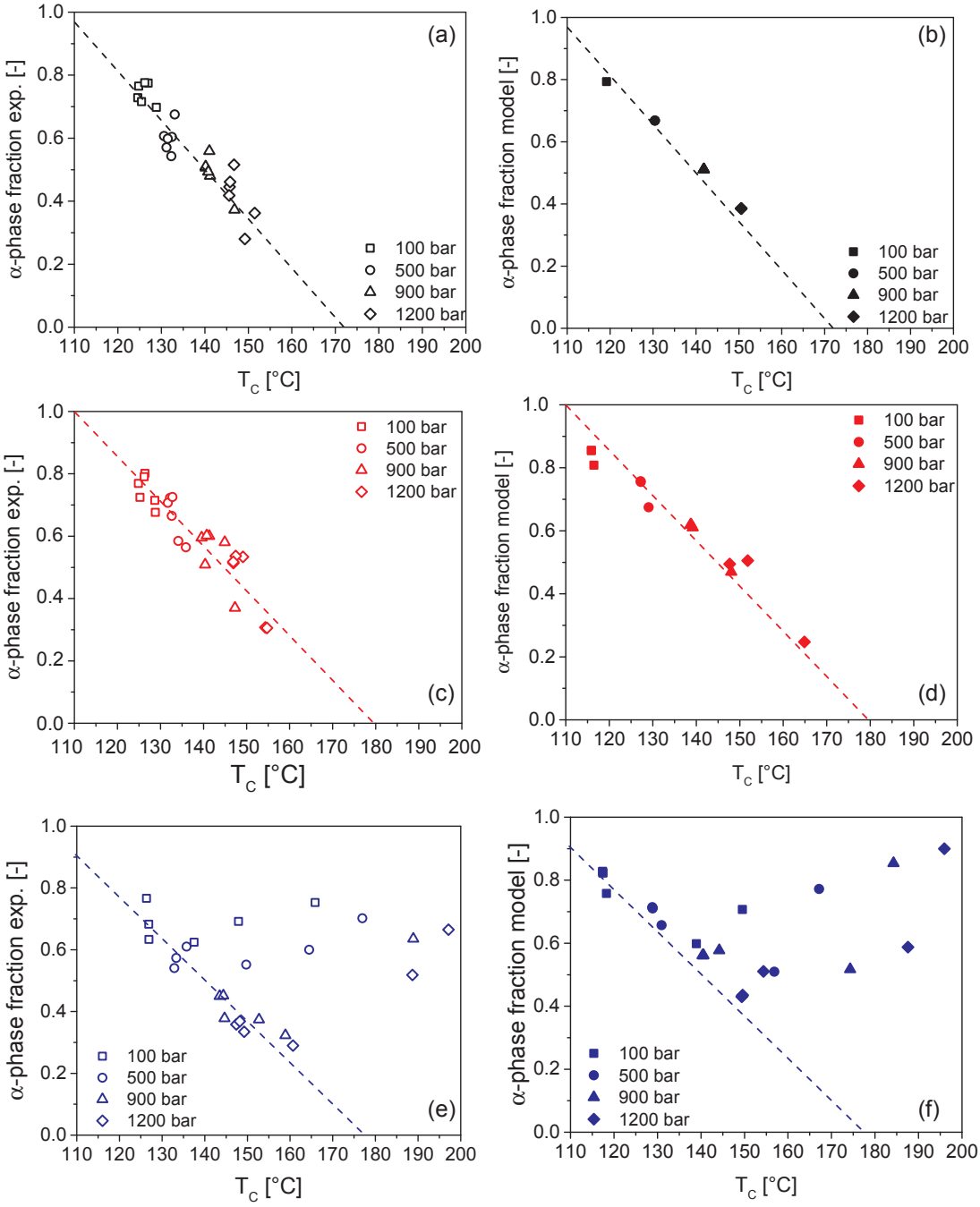

Fig. 6. α-phase volume fraction as a function of the crystallization temperature (T_c) for the LMW (a, b), bimodal (c, d) and HMW (e, f) materials. Left column (a, c, e) shows experimentally measured values and right column the model predictions (b, d, f). The dashed line is a guide to the eye.

Fig. 8 where the model predictions are shown for the three different materials.

Surprisingly, none of the 60 samples showed presence of β-phase in our experiments. We point out that the highest predicted amount of β-phase is found mostly at low pressure (100–500 bar) and relatively high undercooling (low crystallization T), meaning that this will not significantly affect the big discrepancies found for the amount of α-phase predicted at low undercooling (Figs. 6 and 7). It will actually slightly improve the agreement between experiments and model predictions for low crystallization T. A possible reason for the absence of β-phase could be that β-phase growth in metallocene iPPs is unfavoured. At the moment, no solid explanation can be given to the experimental observations, since very little work has been done on β-phase crystallization of metallocene isotactic polypropylene (for example using nucleating agents or flow fields to induce it).

Choi and White [60] found substantial amounts of β-phase (up to 15%) in metallocene iPPs with rather low tacticity obtained by melt spinning.

De Rosa et al. investigated the crystallization behavior of isotactic polypropylene from metallocene catalysis and different stereo-regularity [8] and comonomer content [9] and found an increase in the amount of γ-form with decreasing the average length of isotactic sequences or with increasing comonomer content.

Krache et al. studied the effect of cooling rate on the crystallization behavior of β-nucleated metallocene iPPs (with 94% of [mmmm] pentads and about 1% of regio errors) and compared it to that of a standard Ziegler-Natta material [61]. They found that the addition of $1\%_{wt}$ of a typical β-nucleating agent to the metallocene iPP was not

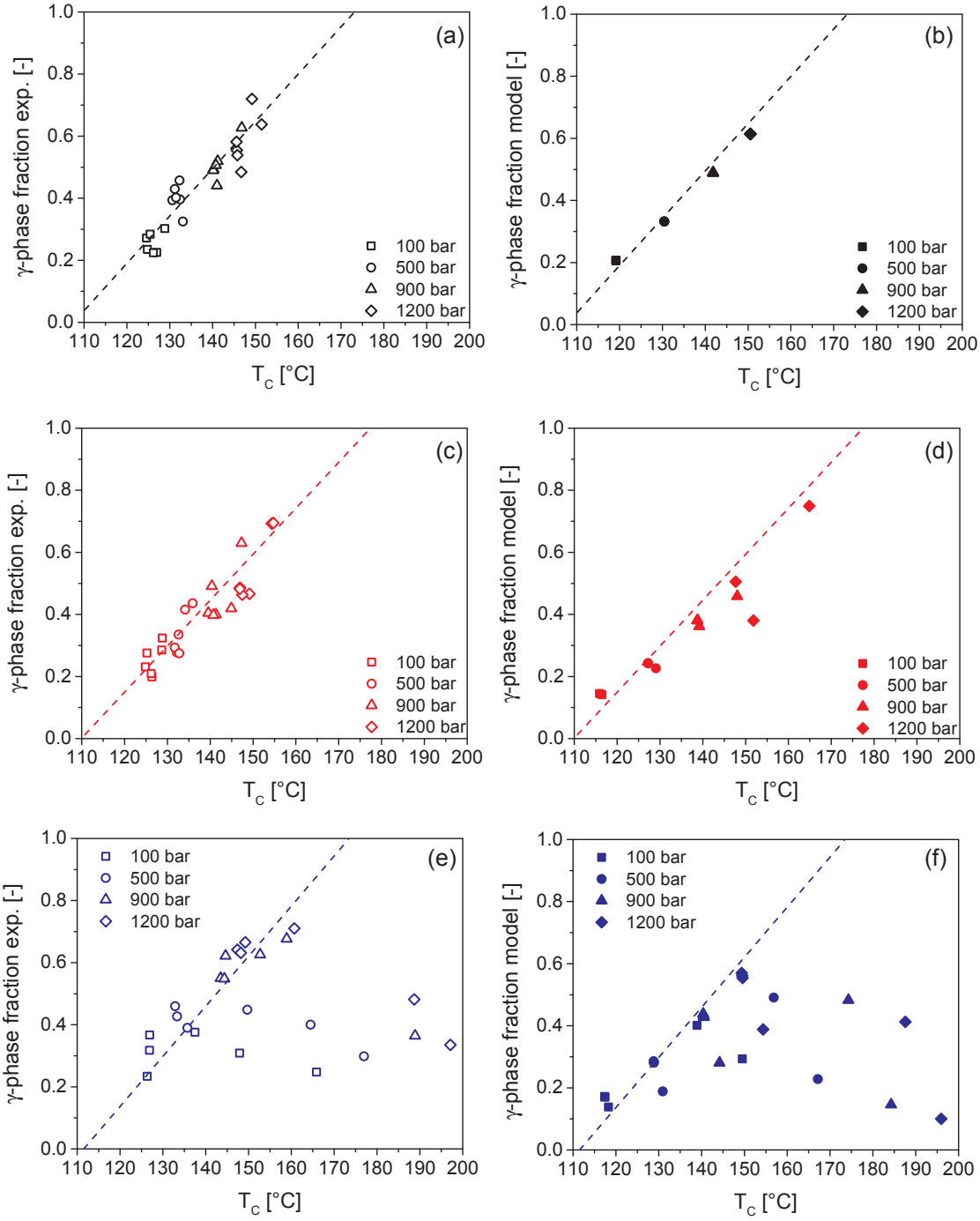

Fig. 7. γ-phase volume fraction as a function of the crystallization temperature (T_c) for the LMW (a, b), bimodal (c, d) and HMW (e, f) materials. Left column (a, c, e) shows experimentally measured values and right column the model predictions (b, d, f). The dashed line is a guide to the eye.

enough to develop any appreciable amount of β-phase in a broad range of cooling rates (2–200 °C/min), whereas the same amount added to the Ziegler-Natta polymer led to 100% of the β modification at low cooling rates. Their speculation was that such amount of nucleating agent was not enough to counterbalance the well known γ formation at relatively high content of defects (stereo- and regio-errors).

A plausible explanation to our experimental observations would be that, although flow might form some β nuclei, their growth, for metallocene systems, is so much slower if compared to the ones of α and γ-phase that they can hardly fill any space, resulting in a concentration which is below the X-ray detection limit.

5. Conclusions and outlook

The flow induced crystallization behavior at elevated pressure was characterized for a set of isotactic polypropylenes from metallocene catalysis, having different molecular weight and molecular weight distributions (relatively low, bimodal and high molecular weight). A unique dilatometer device able to apply shear flow to the polymer melt was used and the effect of flow on crystallization was quantified measuring the shift of the crystallization temperature and the samples were analyzed ex-situ using X-ray diffraction technique to measure the different crystal phases formed.

We used this dataset, consisting of 60 different experiments, as a test

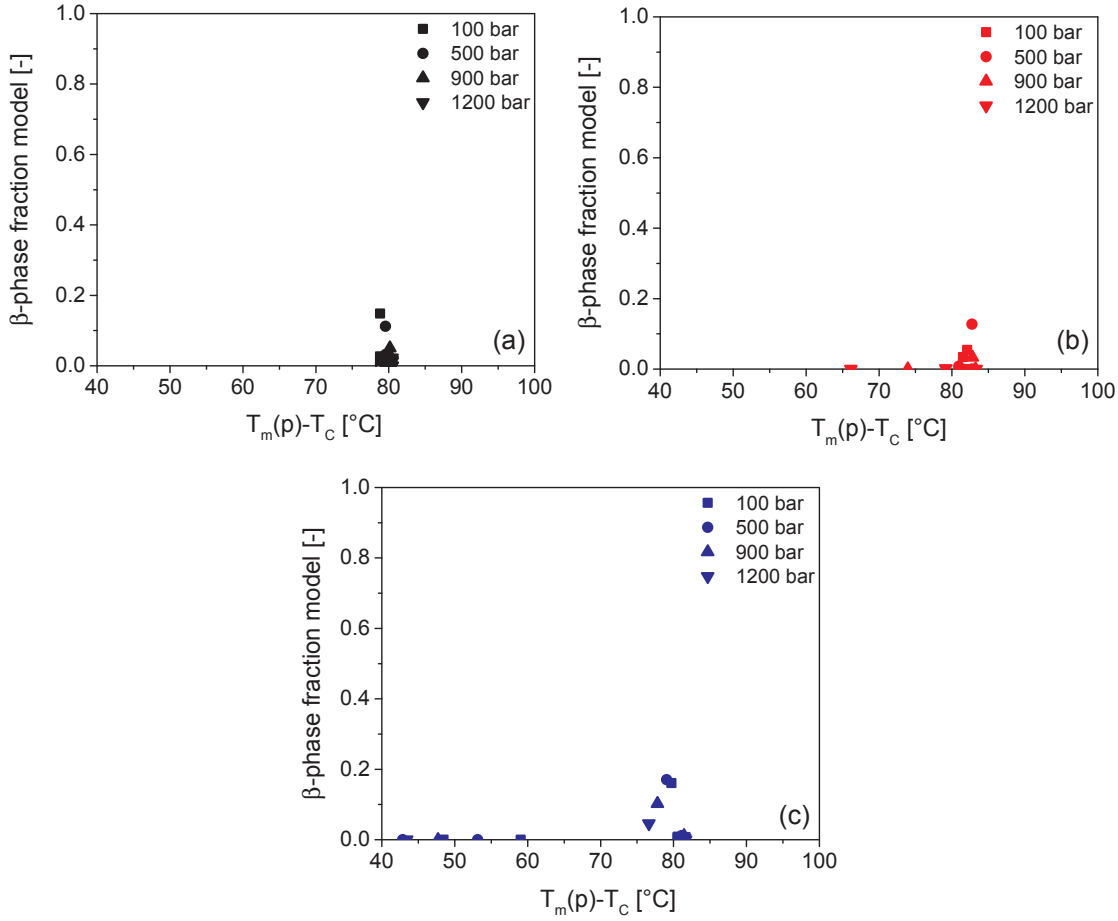

Fig. 8. Model predictions for the β-phase volume fraction as a function of the pressure corrected undercooling for the LMW (a), bimodal (b) and HMW (c) materials.

bed for a previously developed numerical model [33] which includes the effect of flow and pressure on the crystallization behavior and which was used, so far, only on a single Ziegler-Natta iPP.

Only the functions describing the temperature dependence of the quiescent nucleation densities and growth rate were tuned using experimentally measured values and a pre-factor related to the fraction of chains representative of the longest relaxation mode was introduced in the equation for the formation of flow-induced nuclei solely for the bimodal material.

The model prediction of the crystallization temperatures and of the volume fractions of the α and γ polymorphs showed reasonably good agreement with the experimental data, fully capturing the observed trends.

Surprisingly, none of the experiments showed the presence of β-phase whereas the model, assigning a fixed amount of nuclei created by flow to this crystal modification, predicts amounts as high as 20% for certain flow conditions. Although at the moment, no clear explanation can be given to the experimental evidence (more experiments are needed), a possible explanation could be given by a lower growth rate of the β-phase in metallocene systems, which present higher amount of regio-errors (2,1 insertion) if compared to the classical Ziegler-Natta object of the previous studies.

Acknowledgements

EMT is grateful to Marco Hendrix (TU Eindhoven) for the experimental support for the wide angle X-ray diffraction measurements. AHT would like to acknowledge experimental supports provided by Steve Brown, Shuhui Kang, Carlos Lopez-Barron, Hillary Passino, and Sarah Mattler of ExxonMobil Chemical.

Appendix A. Supplementary material

Supplementary data associated with this article can be found, in the online version, at http://dx.doi.org/10.1016/j.eurpolymj.2017.09.042.

References

[1] G. Natta, P. Corradini, Structure and properties of isotactic polypropylene, Il Nuovo Cimen. Ser. 10 15 (1 Supplement) (1960) 40–51.
[2] V.H.J. Leugering, Einfluß der kristallstruktur und der überstruktur auf einige eigenschaften von polypropylen, Die Makromol. Chem. 109 (1) (1967) 204–216.
[3] J. Varga, I. Mudra, G.W. Ehrenstein, Highly active thermally stable β-nucleating agents for isotactic polypropylene, J. Appl. Polym. Sci. 74 (10) (1999) 2357–2368.
[4] C. Mathieu, A. Thierry, J.C. Wittmann, B. Lotz, Specificity and versatility of nucleating agents toward isotactic polypropylene crystal phases, J. Polym. Sci., Part B: Polym. Phys. 40 (22) (2002) 2504–2515.
[5] J. Varga, J. Karger-Kocsis, Rules of supermolecular structure formation in sheared isotactic polypropylene melts, J. Polym. Sci., Part B: Polym. Phys. 34 (4) (1996) 657–670.
[6] K. Mezghani, P.J. Phillips, The γ-phase of high molecular weight isotactic polypropylene. ii: The morphology of the γ-form crystallized at 200 mpa, Polymer 38 (1997) 5725–5733.
[7] C. Angelloz, R. Fulchiron, A. Douillard, B. Chabert, R. Fillit, A. Vautrin, L. David, Crystallization of isotactic polypropylene under high pressure: γ-phase, Macromolecules 33 (1) (2000) 4138–4145.
[8] C. De Rosa, F. Auriemma, A. Di Capua, L. Resconi, S. Guidotti, I. Camurati, I.E. Nifant'ev, I.P. Laishevtsev, Structure-property correlations in polypropylene from metallocene catalysts: Stereodefective, regioregular isotactic polypropylene, J. Am. Chem. Soc. 126 (51) (2004) 17040–17049.
[9] C. De Rosa, F. Auriemma, O.R. De Ballesteros, L. Resconi, I. Camurati, Crystallization behavior of isotactic propylene-ethylene and propylene-butene copolymers: Effect of comonomers versus stereodefects on crystallization properties of isotactic polypropylene, Macromolecules 40 (18) (2007) 6600–6616.
[10] R.G. Alamo, M.-H. Kim, M.J. Galante, J.R. Isasi, L. Mandelkern, Structural and kinetic factors governing the formation of the γ-polymorph of isotactic polypropylene, Macromolecules 32 (12) (1999) 4050–4064.
[11] A. Turner-Jones, Development of the γ-crystal form in random copolymers of

propylene and their analysis by dsc and x-ray methods, Polymer 12 (8) (1971) 487–508.
[12] P. Corradini, V. Petraccone, C. De Rosa, G. Guerra, On the structure of the quenched mesomorphic phase of isotactic polypropylene, Macromolecules 19 (11) (1986) 2699–2703.
[13] C. De Rosa, S. Dello Iacono, F. Auriemma, E. Ciaccia, L. Resconi, Crystal structure of isotactic propylene-hexene copolymers: the trigonal form of isotactic polypropylene, Macromolecules 39 (18) (2006) 6098–6109.
[14] B. Lotz, A new ϵ crystal modification found in stereodefective isotactic polypropylene samples, Macromolecules 47 (21) (2014) 7612–7624.
[15] R. Androsch, M.L. Di Lorenzo, C. Schick, B. Wunderlich, Mesophases in polyethylene, polypropylene, and poly(1-butene), Polymer 51 (21) (2010) 4639–4662.
[16] A. Keller, H.W.H. Kolnaar, Flow-Induced Orientation and Structure Formation, Wiley VCH, 1997 chapter 4, pp. 189–266.
[17] G. Kumaraswamy, R.K. Verma, J.A. Kornfield, F. Yeh, B.S. Hsiao, Shear-enhanced crystallization in isotactic polypropylene. in-situ synchrotron saxs and waxd, Macromolecules 37 (24) (2004) 9005–9017.
[18] Z. Ma, L. Balzano, G. Portale, G.W.M. Peters, Flow induced crystallization in isotactic polypropylene during and after flow, Polymer 55 (23) (2014) 6140–6151.
[19] P.C. Roozemond, Z. Ma, K. Cui, L. Li, G.W.M. Peters, Multimorphological crystallization of shish-kebab structures in isotactic polypropylene: quantitative modeling of parent-daughter crystallization kinetics, Macromolecules 47 (15) (2014) 5152–5162.
[20] T.B. van Erp, L. Balzano, G.W.M. Peters, Oriented gamma phase in isotactic polypropylene homopolymer, ACS Macro Lett. 1 (5) (2012) 618–622.
[21] J.W. Housmans, M. Gahleitner, G.W.M. Peters, H.E.H. Meijer, Structure-property relations in molded, nucleated isotactic polypropylene, Polymer 50 (10) (2009) 2304–2319.
[22] G. Kalay, M.J. Bevis, Processing and physical property relationships in injection-molded isotactic polypropylene. 2. Morphology and crystallinity, J. Polym. Sci., Part B: Polym. Phys. 35 (2) (1997) 265–291.
[23] H.E.H. Meijer, L.E. Govaert, Mechanical performance of polymer systems: the relation between structure and properties, Prog. Polym. Sci. 30 (8–9) (2005) 915–938.
[24] Gerhard Eder, Hermann Janeschitz-Kriegl, Crystallization, Chapter Structure Development During Processing, Wiley VCH Verlag GmbH & Co. KGaA, 2006.
[25] H. Zuidema, G.W.M. Peters, H.E.H. Meijer, Development and validation of a recoverable strain-based model for flow-induced crystallization of polymers, Macromol. Theory Simul. 10 (5) (2001) 447–460.
[26] F.J.M.F. Custodio, R.J.A. Steenbakkers, P.D. Anderson, G.W.M. Peters, H.E.H. Meijer, Model development and validation of crystallization behavior in injection molding prototype flows, Macromol. Theory Simul. 18 (9) (2009) 469–494.
[27] M. van Drongelen, T.B. van Erp, G.W.M. Peters, Quantification of non-isothermal, multi-phase crystallization of isotactic polypropylene: the influence of cooling rate and pressure, Polymer 53 (21) (2012) 4758–4769.
[28] T.B. van Erp, P.C. Roozemond, G.W.M. Peters, Flow-enhanced crystallization kinetics of ipp during cooling at elevated pressure: characterization, validation, and development, Macromol. Theory Simul. 22 (5) (2013) 309–318.
[29] P.C. Roozemond, M. van Drongelen, Z. Ma, M.A. Hulsen, G.W.M. Peters, Modeling flow-induced crystallization in isotactic polypropylene at high shear rates, J. Rheol. 59 (3) (2015) 613–642.
[30] M. van Drongelen, P.C. Roozemond, E.M. Troisi, A.K. Doufas, G.W.M. Peters, Characterization of the primary and secondary crystallization kinetics of a linear low-density polyethylene in quiescent- and flow-conditions, Polymer 76 (2015) 254–270.
[31] W. Schneider, A. Köppl, J. Berger, Non-isothermal crystallization of polymers, Int. Polym. Process. 2 (3–4) (1988) 151–154.
[32] M. Avrami, Kinetics of phase change. i. General theory, J. Chem. Phys. 7 (12) (1939) 1103–1112.
[33] P.C. Roozemond, T.B. van Erp, G.W.M. Peters, Flow-induced crystallization of isotactic polypropylene: modeling formation of multiple crystal phases and morphologies, Polymer 89 (2016) 69–80.
[34] M.H.E. Van der Beek, G.W.M. Peters, H.E.H. Meijer, Influence of shear flow on the specific volume and the crystalline morphology of isotactic polypropylene, Macromolecules 39 (5) (2006) 1805–1814.
[35] T.B. van Erp, L. Balzano, A.B. Spoelstra, L.E. Govaert, G.W.M. Peters, Quantification of non-isothermal, multi-phase crystallization of isotactic polypropylene: the influence of shear and pressure, Polymer 53 (25) (2012) 5896–5908.
[36] Dario Cavallo, Fiorenza Azzurri, Roberto Floris, Giovanni C. Alfonso, Luigi Balzano, Gerrit W. Peters, Continuous cooling curves diagrams of propene/ethylene random copolymers. the role of ethylene counits in mesophase development, Macromolecules 43 (6) (2010) 2890–2896.
[37] R. Clausius, Ueber die bewegende kraft der wrme und die gesetze, welche sich daraus fr die wrmelehre selbst ableiten lassen, Ann. Phys. 155 (4) (1850) 500–524.
[38] J. He, P. Zoller, Crystallization of polypropylene, nylon-66 and poly(ethylene terephthalate) at pressures to 200 MPa: kinetics and characterization of products, J. Polym. Sci., Part B: Polym. Phys. 32 (6) (1994) 1049–1067.
[39] A.T. Jones, J.M. Aizlewood, D.R. Beckett, Crystalline forms of isotactic polypropylene, Die Makromol. Chem. 75 (1) (1964) 134–158.
[40] W.M.H. Verbeeten, G.W.M. Peters, F.P.T. Baaijens, Differential constitutive equations for polymer melts: the extended pom-pom model, J. Rheol. 45 (4) (2001) 823–843.
[41] M. Seki, D.W. Thurman, J.P. Oberhauser, J.A. Kornfield, Shear-mediated crystallization of isotactic polypropylene: the role of long chain-long chain overlap, Macromolecules 35 (7) (2002) 2583–2594.
[42] R.H. Somani, B.S. Hsiao, A. Nogales, S. Srinivas, A.H. Tsou, I. Sics, F.J. Balta-Calleja, T.A. Ezquerra, Structure development during shear flow-induced crystallization of i-pp: in-situ small-angle x-ray scattering study, Macromolecules 33 (25) (2000) 9385–9394.
[43] R.R. Lagasse, B. Maxwell, An experimental study of the kinetics of polymer crystallization during shear flow, Polym. Eng. Sci. 16 (3) (1976) 189–199.
[44] P. Jerschow, H. Janeschitz-Kriegl, The role of long molecules and nucleating agents in shear induced crystallization of isotactic polypropylenes, Int. Polym. Process. 12 (1) (1997) 72–77.
[45] S. Vleeshouwers, H.E.H. Meijer, A rheological study of shear induced crystallization, Rheol. Acta 35 (5) (1996) 391–399.
[46] J. van Meerveld, G.W.M. Peters, Markus Hütter, Towards a rheological classification of flow induced crystallization experiments of polymer melts, Rheol. Acta 44 (2) (2004) 119–134.
[47] S. Kimata, T. Sakurai, Y. Nozue, T. Kasahara, N. Yamaguchi, T. Karino, M. Shibayama, J.A. Kornfield, Molecular basis of the shish-kebab morphology in polymer crystallization, Science 316 (5827) (2007) 1014–1017.
[48] M. Doi, S.F. Edwards, The Theory of Polymer Dynamics, Clarendon Press, Oxford, U.K., 1986.
[49] S.E. Kadijk, B.H.A.A. Van Den Brule, On the pressure dependency of the viscosity of molten polymers, Polym. Eng. Sci. 34 (20) (1994) 1535–1546.
[50] R. Cardinaels, P. Van Puyvelde, and P. Moldenaers, Evaluation and comparison of routes to obtain pressure coefficients from high-pressure capillary rheometry data, Rheol. Acta 46 (4) (2007) 495–505.
[51] H. Janeschitz-Kriegl, E. Ratajski, H. Wippel, The physics of athermal nuclei in polymer crystallization, Colloid Polym. Sci. 277 (2) (1999) 217–226.
[52] M. Stadlbauer, H. Janeschitz-Kriegl, G. Eder, E. Ratajski, New extensional rheometer for creep flow at high tensile stress. part ii. Flow induced nucleation for the crystallization of ipp, J. Rheol. 48 (3) (2004) 631–639.
[53] J. Berger, A. Köppl, W. Schneider, Non-isothermal crystallization. Crystallization of polymers. system of rate equations, Int. Polym. Process. 2 (1988) 151–154.
[54] S.Z.D. Cheng, J.J. Janimak, A. Zhang, H.N. Cheng, Regime transitions in fractions of isotactic polypropylene, Macromolecules 23 (1) (1990) 298–303.
[55] J.J. Janimak, S.Z.D. Cheng, P.A. Giusti, E.T. Hsieh, Isotacticity effect on crystallization and melting in poly(propylene) fractions. 2. Linear crystal growth rate and morphology study, Macromolecules 24 (9) (1991) 2253–2260.
[56] M. Gahleitner, C. Bachner, E. Ratajski, G. Rohaczek, W. Neßl, Effects of the catalyst system on the crystallization of polypropylene, J. Appl. Polym. Sci. 73 (12) (1999) 2507–2516.
[57] J.D. Hoffman, Theoretical aspects of polymer crystallization with chain folds: bulk polymers, SPE Trans. 4 (1964) 315–362.
[58] F.G. Hamad, R.H. Colby, S.T. Milner, Lifetime of flow-induced precursors in isotactic polypropylene, Macromolecules 48 (19) (2015) 7286–7299.
[59] L. Fernandez-Ballester, D.W. Thurman, W. Zhou, J.A. Kornfield, Effect of long chains on the threshold stresses for flow-induced crystallization in ipp: shish kebabs vs sausages, Macromolecules 45 (16) (2012) 6557–6570.
[60] K.-J. Choi, J.E. Spruiell, J.L. White, Orientation and morphology of high-density polyethylene film produced by the tubular blowing method and its relationship to process conditions, J. Polym. Sci. Polym. Phys. Ed. 20 (1) (1982) 27–47.
[61] R. Krache, R. Benavente, J.M. López-Majada, J.M. Perena, M.L. Cerrada, E. Pérez, Competition between α, β, and γ polymorphs in a β-nucleated metallocenic isotactic polypropylene, Macromolecules 40 (19) (2007) 6871–6878.